J Therm Anal Calorim (2012) 107:439–445
DOI 10.1007/s10973-011-1656-9

Thermal decomposition of hydromagnesite

Effect of morphology on the kinetic parameters

D. Bhattacharjya · T. Selvamani · Indrajit Mukhopadhyay

Received: 31 December 2010 / Accepted: 11 May 2011 / Published online: 24 July 2011

Abstract Non isothermal decomposition of synthetically prepared hydromagnesite phase with two different morphologies (2-D micro sheets and nests) was studied in dynamic nitrogen atmosphere by thermogravimetric analysis, differential thermogravimetric analysis, and differential scanning calorimetric techniques. Two different kinetic models, i.e. the Friedman isoconversion and the Flynn–Wall methods were employed for the analysis of thermal decomposition. The apparent activation energy (E_a) of the hydromagnesite phases having 2-D micro sheet and nest morphology were calculated and compared. The activation energy of nest morphology was found to be relatively higher than 2-D micro sheets. The higher activation energy for the relatively close packed 'nest' morphology is attributed to the difficulty of thermal transport in the core.

Keywords Synthetic hydromagnesite · Micro-sheets · Non-isothermal decomposition · Arrhenius equation · Activation energy

Electronic supplementary material The online version of this article (doi:10.1007/s10973-011-1656-9) contains supplementary material, which is available to authorized users.

D. Bhattacharjya · T. Selvamani · I. Mukhopadhyay (✉)
Central Salt and Marine Chemicals Research Institute (CSIR), G. B. Marg, Bhavnagar 364002, Gujarat, India
e-mail: indrajit.m@pdpu.ac.in

Present Address:
I. Mukhopadhyay
School of Solar Energy, Pandit Deendayal Petroleum University, Raisan, Gandhinagar 382007, Gujarat, India

Introduction

Basic magnesium carbonates, with the general formula $xMgO{\cdot}yCO_2{\cdot}zH_2O$ are important class of compounds which find assorted industrial applications [1]. Hydromagnesite, $Mg_5[(CO_3)_4(OH)_2]{\cdot}4H_2O$, the most commonly available magnesium hydroxy carbonate, has also several useful applications. It is largely used as an inert vehicle, an ingredient for tooth pastes and an active adsorbent in the pharmaceutical industry. Owing to its fine texture and high absorbency, it is used in cosmetics as a carrier and retainer of perfumes. In the rubber industry, hydromagnesite is used as a reinforcing agent. It is also used as an extender instead of TiO_2 in the paint industry [2]. It can also be used as a precursor for the synthesis of other magnesium-based materials [2–5]. Hydromagnesite is also a well-known bridging component in ancient magnesian lime mortars [6]. Thermal decomposition of hydromagnesite is usually associated with an endothermic break down in the temperature range of 200–550 °C. This process is associated with a heat of decomposition of 800 Jg^{-1} which enables hydromagnesite as an important fire retardant agent [3, 7]. Besides its natural abundance, a number of chemical methods namely hydrothermal syntheses, carbonation and precipitation have been developed to produce hydromagnesite [4, 8–11]. Since the fire retardant properties are directly related to the particle size and its morphology, a number of wet chemical routes have been proposed for the preparation of synthetic hydromagnesite of definite shape in low dimensions [4, 12].

Non isothermal decomposition kinetics of solids has been studied extensively [13–17]. Various techniques are available for deducing the kinetic parameters for the thermal conversions involving solids and exploring the reaction mechanism [18–23]. It has already been established

that the reliability of the results obtained by model-free method for thermal degradation kinetics such as the Friedman isoconversion method, Flynn–Wall Method, Kissinger Method are far superior to that obtained by other model fitting approach such as the differential method [16, 17, 24]. Thermal decomposition of hydromagnesite has also been studied [3, 17, 25, 26]. Thermal decomposition of hydromagnesite in air has been described by the following reactions [7]:

$$Mg_5(CO_3)_4(OH)_2 \cdot 4H_2O \rightarrow Mg_5(CO_3)_4 \cdot Mg(OH)_2 + 4H_2O \ (<250\ ^\circ C)$$

$$Mg_5(CO_3)_4 \cdot Mg(OH)_2 \rightarrow Mg_4(CO_3)_4 + MgO + H_2O \ (250-350\ ^\circ C)$$

$$Mg_4(CO_3)_4 \rightarrow 4MgO + 4CO_2 \ (>350\ ^\circ C)$$

However, it has been found that increase in sample size and heating rate beyond a typical limit changes the decomposition mechanism of hydromagnesite with the occurrence of an exotherm at around 520 °C followed by a third endotherm [26]. Similar observation has also been made when the thermal decomposition is carried out in CO_2 atmosphere [27]. Though many studies on the decomposition of hydromagnesite have been carried out in the past, no exploratory work is found to deal with the dependence of the kinetics of decomposition on the morphology of the hydromagnesite phase.

In this communication the authors report on the analysis of kinetics for the thermal decomposition of synthetic hydromagnesites which exist in two different morphologies (micro-sheet and close packed nest) in dynamic nitrogen atmosphere. The hydromagnesite phases were prepared by controlled hydrothermal and simple precipitation process using $MgCl_2$ precursor [28, 29]. The kinetic parameters were deduced by the model-free Friedman isoconversion and Flynn–Wall method. The dependence of the activation energy on the morphology is described as a function of the degree of conversion (α).

Experimental

Preparation of hydromagnesite with different morphology

Hydromagnesite micro-sheets, used in this study, was synthesized by refulxing $MgCl_2$ in freshly prepared urea solution in the presence of ethylene glycol at 110 ± 10 °C for 12 h in air under continuous magnetic stirring (500 rpm) [28]. Hydromagnesite in nest morphology was prepared by the chemical reaction of $MgCl_2{\cdot}6H_2O$ with Na_2CO_3 solution in aqueous medium using H_2O_2 as internal pressure regulator [29].

Characterization

The as synthesized hydromagnesite phases were characterized by powder X-ray diffraction (XRD) using Cu K_α radiation. The morphology of the products was explored by using field emission scanning electron microscopy (FE-SEM, JEOL JSM-7001FF). Powder samples were put over the conducting carbon tape and coated with thin layer (~4–8 nm) of Au before analysing by FE-SEM. All the thermogravimetry and differential scanning calorimetric studies were carried out on a Mettler Toledo thermogravimetric analyser, models 851^e and 822^e, respectively, under N_2 flow (flow rate of 50 mL min^{-1}). Standard aluminium crucibles were used to analyse the samples. TG experiments were performed using sample size of 5 mg. The range of temperature studied was from 25 to 550 °C, at the heating rates of 5, 7.5, 10, and 12.5 °C min^{-1}.

Theory

The specific rate for a solid state reaction can be defined as

$$\frac{d\alpha}{dt} = kf(\alpha) \quad (1)$$

where t is the time, α is the extent of the reaction (or the fraction decomposed) which can have values in the range of 0–1 and f(α) is some expression associated with the kinetic model of the reaction [13, 14, 16]. For non-isothermal decomposition process, the expression of Eq. 1 can be used in the Arrhenius equation to give an expression:

$$\ln\left(\frac{d\alpha}{dt}\right) = -\frac{E_a}{RT} + \ln[Af(\alpha)] \quad (2)$$

Equation 2 is the expression for the Friedman isoconversion method which avoids the explicit kinetic models, $f(\alpha)$. According to Eq. 2, a plot of $\ln(d\alpha/dt)$ versus $1/T$ for fixed α will be linear, the slope of which will give the values of $(-E_a/R)$ and subsequently, the activation energy E_a. Flynn–Wall method is one of the important model-free methods by which the energy of activation can be calculated according to the following equation [24]:

$$\frac{d\ln\beta}{d\left(\frac{1}{T}\right)} = \left(\frac{10}{e} \times 0.4567\, E_a\right)/R \quad (3)$$

A plot of $\ln\beta$ (β is the heating rate) against $1/T$ will give a straight line, the slope of which can be used to calculate the activation energy.

Result and discussion

Spectroscopy and microscopy

The powder XRD patterns of the as-prepared compounds are shown in Fig. 1. All the diffraction lines can be indexed to the monoclinic hydromagnesite phase (Fig. 1a-i) $Mg_5[(CO_3)_4(OH)_2]\cdot 4H_2O$ with no unwanted impurity peaks [28]. The sharp peaks in Fig. 1a-i indicates relatively higher crystallinity of the corresponding hydromagnesite phase. The morphology of the hydromagnesite phases are shown in Fig. 1b–d. The hydromagnesite phase obtained by hydrothermal method exists in 2-D rectangular sheet morphology (Fig. 1b, c). It can be noticed that the sheets are ordered and rectangular in shape with side length in the range of 2–2.5 μm and an apparent thickness of 15–20 nm [28]. The two dimensional sheets are also stacked in three dimensions. However, as shown in Fig. 1d, the simple precipitation technique leads to the formation of hydromagnesite phase in spherical nest like morphology [29]. Each nest is formed by ordered assembly of layered hydromagnesite scales in a compact way. The spherical nests are 10–15 μm in diameter.

Thermal analysis

The TG and DTG profile for the decomposition of hydromagnesite sheets at various heating rates is shown in

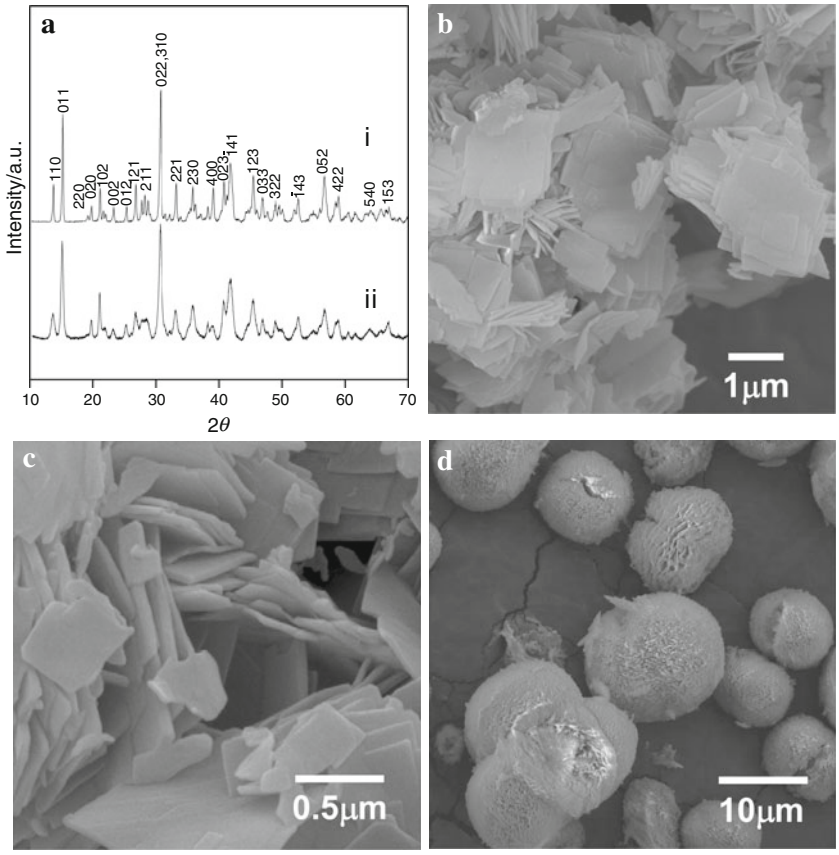

Fig. 1 **a** XRD patterns of synthetically prepared hydromagnesite phases with *i* spherical nest and *ii* 2-D sheet morphology obtained by precipitation and hydrothermal syntheses, respectively; SEM images of (**b**, **c**) hydromagnesite sheets and **d** spherical nest

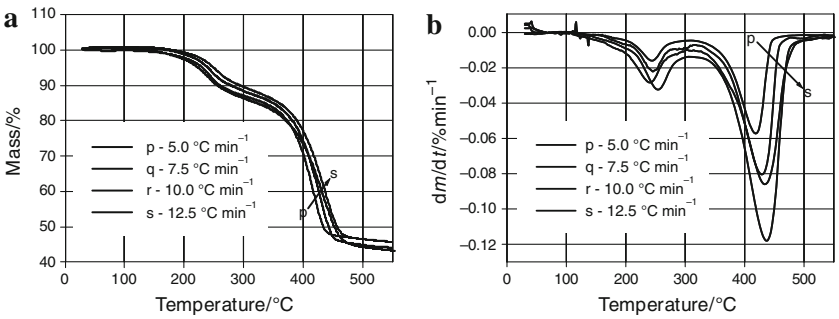

Fig. 2 **a** TG and **b** DTG profiles for the thermal decomposition of hydromagnesite sheets at various heating rates in dynamic N_2 atmosphere (sample size 5 mg)

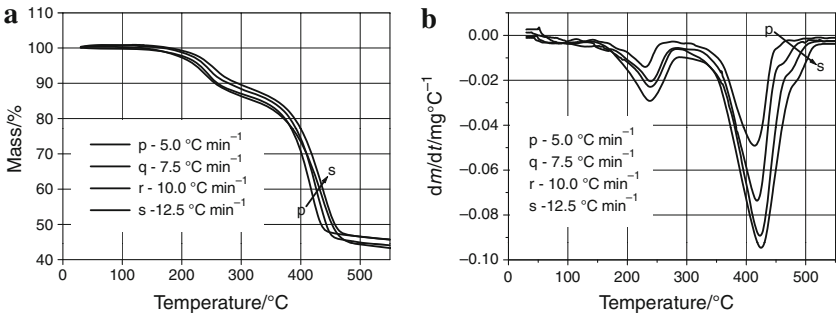

Fig. 3 **a** TG and **b** DTG profiles for the thermal decomposition of hydromagnesite nests at various heating rates in dynamic N_2 atmosphere (sample size 5 mg)

Table 1 Comparison of thermogravimatric data of different hydromagnesite phases

Sample	β/°C min^{-1}	30–300 °C		300–550 °C	
		mass/%	T_p/°C	mass/%	T_p/°C
Hyd. sheet	5	13.08	244.5	41.36	418.6
	7.5	11.80	245	44.29	429.0
	10	13.86	240	44.03	434.8
	12.5	10.79	254	43.82	437.3
Hyd. flower	5	13.14	229.8	41.10	414
	7.5	15.68	239	42.36	418.5
	10	13.19	239	42.76	423
	12.5	12.15	238.3	41.54	425
Commercial Hyd.[a]	10	17.90	227	38.30	417.8

[a] Grounded commercial hydromagnesite [30]

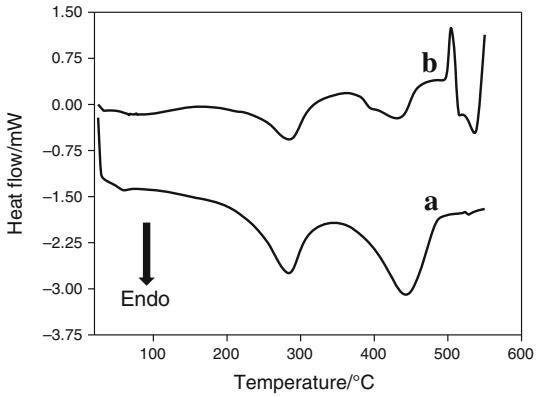

Fig. 4 DSC heat flow patterns of hydromagnesite **a** 2-D sheets and **b** nests using sample size of 5 mg at a heating rate of 10 °C min^{-1} in N_2

Fig. 2. Two prominent mass loss steps are observed in the temperature range of 200–300 and 300–500 °C. The first mass loss is ca. 13.86% while the second loss is equal to 44.04% of the initial mass when the measurements were carried out at a heating rate of 10 °C min^{-1}. The total mass loss of 57.90% is found to be close to the theoretical mass loss expected from hydromagnesite phase [5]. It can be noted from Fig. 2 that the decarbonation step occurring at the temperature range of 300–500 °C is one of the major thermal events in hydromagnesite. However, the dehydroxylation step is found to overlap both with the dehydration and decarbonation steps [14]. The DTG profile shown in Fig. 2b shows continuous shift of the peak temperature for both the dehydration–dehydroxylation and decarbonation steps towards the higher value. The TG and DTG profiles for the hydromagnesite phase with spherical nest morphology are shown in Fig. 3. The nature of the profiles are similar to that of Fig. 2. The total mass loss is close to 56.3% confirming the spherical nest particles as hydromagnesite. However, a clear differences in the nature of temperature shift for the decarbonation step in Figs. 2b and 3b is noticed. As shown in Table 1, the shift of peak temperature (T_p) for the decarbonation step is more prominent for hydromagnesite sheets than the nest analogue. This observation can be attributed to the efficient heat transfer in the sheets than that in hydromagnesite spherical nests at higher heating rates [27].

The DSC profiles in Fig. 4a indicate two distinct endothermic processes occurring in the temperature range of 200–300 and 300–500 °C for hydromagnesite with sheet morphology. However, the diffuse character of the peaks clearly indicates overlapping of the dehydroxylation step with the dehydration and decarbonation steps [14]. The DSC profile thus supports the TG curve in Fig. 2 where the mass loss due to dehydration and dehydroxylation is registered in a single mass loss step. The heat of decomposition of the hydromagnesite phase with sheet morphology is found to be 860 J g^{-1}. In the case of hydromagnesite nests, an exothermic peak is observed along with three endothermic peaks (Fig. 4b). The exothermic peak has been attributed to the crystallization of magnesite ($MgCO_3$) from amorphous intermediates during the thermal decomposition process [30]. But, in the present case the authors do not observe any abrupt increase in the mass loss. Hence, the authors can infer that the self generated CO_2 enhances CO_2 partial pressure inside the stable nest morphology and is responsible for exhibiting the difference in the DSC profiles [1, 27, 30]. The net enthalpy of decomposition,

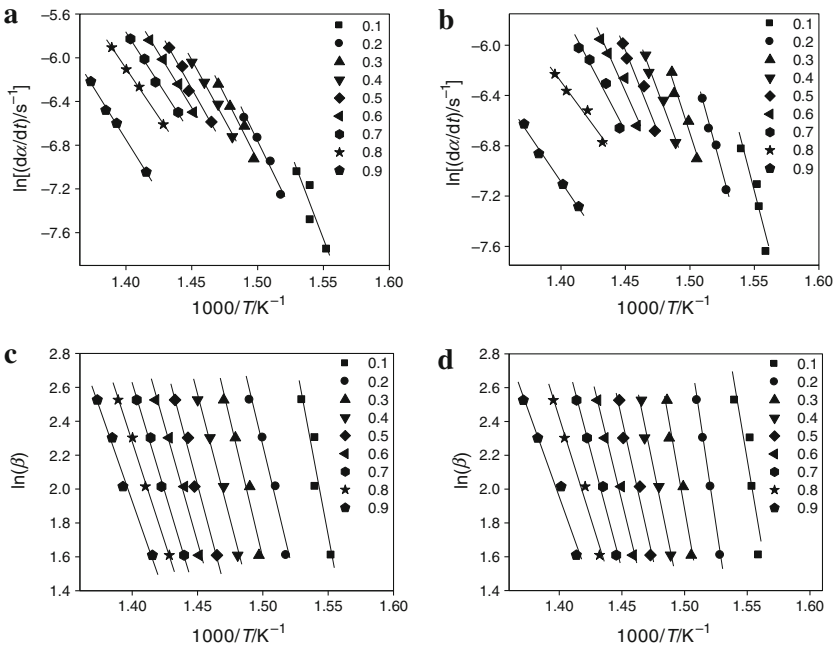

Fig. 5 Friedman isoconversion plots for hydromagnesite phase with **a** 2-D sheets and **b** nest morphology; the Flynn–Wall plots for **c** 2-D sheet and **d** nest

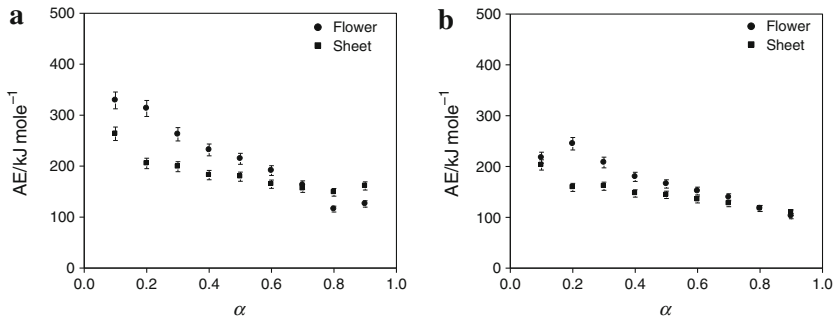

Fig. 6 Variation of activation energy with α for hydromagnesite phase with (*filled square*) 2-D sheet and (*filled circle*) nest morphology as per **a** Friedman and **b** Flynn–Wall method

however, found to be much lower ($\sim$536 kJ mol^{-1}) than hydromagnesite sheets.

The kinetic of non-isothermal decomposition of hydromagnesite phase with two different morphologies were analyzed using TG data acquired at various heating rates by Friedman isoconversion and Flynn–Wall methods. Both the methods avoid use of any explicit kinetic model (sample size 5.0 mg, data of Figs. 2a and 3a). The effect of overlapping of the dehydroxylation step with the decarbonation step in both the samples is assumed to be identical. In the kinetic analysis the authors have considered the decarbonation step only as it constitutes the major thermal event in the whole decomposition process of hydromagnesite. Typical Friedman isoconversion plots for the decarbonation step of hydromagnesite phase with two different morphologies at various α are presented in Fig. 5a, b. It can be seen from the Fig. 5a, b that the hydromagnesite phases with sheet and spherical nest morphologies provide rather good linear fits at constant α values ranging from 0.2 to 0.9. The fitting parameter is not so good for $\alpha = 0.1$. The Flynn–Wall plots for the hydromagnesite phase with different morphologies are shown is Fig. 5c, d. The variation of activation energies with α for two different hydromagnesite microstructures is shown in Fig. 6. It is observed that the activation energy of the hydromagnesite phase with sheet type morphology is lower than the hydromagnesite phase with the nest type morphology. However, the activation energy for both the samples is not constant and varies with the extent of conversion α indicating that the thermal decomposition of hydromagnesite is a complicated multi step process characterized by different activation energy in different temperature ranges involving different reaction mechanism. The mean activation energy, obtained by isoconversional method, for hydromagnesite with sheet and nest morphologies is found to be 174 and 202 kJ mol^{-1}, respectively, in the region of $0.2 \leq \alpha \leq 0.9$. Similar trend of variation of activation energy is also observed when Flynn–Wall method is employed. However, the absolute value of activation energies decreased. It is interesting to note that the

activation energy of commercial hydromagnesite phase having aggregates of scales like crystallites is much lower (141 kJ mol^{-1}) than the activation energy of the synthetic hydromagnesite phases with different microstructures [30].

Conclusions

In conclusions the authors have shown that synthetically prepared hydromagnesite decompose in two distinct temperature regions: the dehydration and dehydroxylation takes place in the temperature range of 200–300 °C while the decarbonation occurs in the range of 300–450 °C. The dehydroxylation step is found to overlap both with the dehydration and decarbonation steps. The heat of decomposition of the hydromagnesite sheets is found to be $\geq$860 J gm^{-1} which is relatively higher than commercially available hydromagnesite phase. A strong dependence of the activation energy for the decarbonation step of hydromagnesite to its morphology is found to exist. While the Friedman isoconversion method gives mean-activation energies of 174 and 202 kJ mol^{-1} for hydromagnesite with 2-D micro-sheets and close packed nest morphologies, respectively, the Flynn–Wall method shows the corresponding values as 144 and 169 kJ mol^{-1}. These values are rather higher than the activation energy of commercially available hydromagnesite phase. The larger activation energy of the hydromagnesite nests is attributed to the difficulty in thermal conduction to the core. Also the closed packed nest morphology does not allow easy transport of the decomposed product from the core structure.

Acknowledgements The authors thank Department of Science and Technology (DST) Govt. of India and CSIR for financial support through project no. SR/S1/PC-1/2010 and NWP 0010, respectively.

References

1. Hollingbery LA, Hull TR. The fire retardant behaviour of huntite and hydromagnesite—A review. Polym Degrad Stab. 2010;95:2213–5.
2. Kirk RE, Othmer DF. Encyclopedia of chemical technology, vol. 15. New York: Wiley & Sons; 1995.
3. Haurie L, Fernández AI, Velasco JI, Chimenos JM, Lopez-Cuesta JM, Espiell F. Effects of milling on the thermal stability of synthetic hydromagnesite. Mat Res Bull. 2007;42:1010–8.
4. Yan C, Xue D. Novel self-assembled MgO nanosheet and its precursors. J Phys Chem B. 2005;109:12358–61.
5. Janet CM, Viswanathan B, Viswanath RP, Varadarajan TK. Characterization and photoluminescence properties of MgO microtubes synthesized from hydromagnesite flowers. J Phys Chem C. 2007;111:10267–72.
6. Bruni S, Cariatia F, Fermoa P, Pozzia A, Toniolob L. Characterization of ancient magnesian mortars coming from northern Italy. Thermochim Acta. 1998;321:161–5.
7. Botha A, Strydom CA. Preparation of a magnesium hydroxy carbonate from magnesium hydroxide. Hydrometallurgy. 2001;62:175–83.
8. Choudhary VR, Pataskar SG, Gunjikar VG, Zope GB. Influence of preparation conditions of basic magnesium carbonate on its thermal analysis. Thermochim Acta. 1994;232:95–110.
9. Morie T, Kuroki T, Matsumoto Y. Manufacture of porous spherical basic magnesium carbonate with narrow particle size. 1986; JP86-235240.
10. Yan C, Xue D, Zou L. Fabrication of hexagonal MgO and its precursors by a homogeneous precipitation method. Mat Res Bull. 2006;41:2341–8.
11. Zhang Z, Zheng Y, Zhang J, Zhang Q, Chen J, Liu Z, Liang X. Synthesis and shape evolution of monodisperse basic magnesium carbonate microspheres. Cryst Growth Des. 2007;7:337–42.
12. Li Q, Ding Y, Yu G, Li C, Li F, Qian Y. Fabrication of light-emitting porous hydromagnesite with rosette-like architecture. Solid State Commun. 2003;125:117–20.
13. Burnham AK, Dinh LN. A comparison of isoconversional and model fitting approaches to kinetic parameter estimation and application prediction. J Therm Anal Calorim. 2007;89:479–90.
14. Frost RL, Hales MC, Martens WN. Thermogravimetric analysis of selected group (II) carbonate minerals—implication for the geosequestration of greenhouse gases. J Therm Anal Calorim. 2009;95:999–1005.
15. Vyazovkin S, Sbirrazzuoli N. Isoconversional kinetic analysis of thermally stimulated processes in polymers. Macromol Rapid Commun. 2006;27:1515–32.
16. Budrugeac P, Homentcovschi D, Segal E. Critical analysis of the isoconversional methods for evaluating the activation energy. J Therm Anal Calorim. 2001;63:457–63.
17. Vágvölgyi V, Frost RL, Hales M, Locke A, Kristóf J, Horváth E. Controlled rate thermal analysis of hydromagnesite. J Therm Anal Calorim. 2008;92:893–7.
18. Palmer SJ, Frost RL, Nguyen T. Thermal decomposition of hydrotalcite with molybdate and vanadate anions in the interlayer. J Therm Anal Calorim. 2008;92:879–86.
19. Aphane ME, van der Merwe EM, Strydom CA. Influence of hydration time on the hydration of MgO in water and in a magnesium acetate solution. J Therm Anal Calorim. 2009;96:987–92.
20. Vagvolgyi V, Hales M, Martens W, Kristof J, Horvath E, Frost RL. Dynamic and controlled rate thermal analysis of hydrozincite and smithsonite. J Therm Anal Calorim. 2008;92:911–6.
21. Keuleers RR, Janssens JF, Desseyn HO. Comparison of some methods for activation energy determination of thermal decomposition reactions by thermogravimetry. Thermochim Acta. 2002;385:127–42.
22. Dollimore D, Heal GR, Krupay RW. The use of the rising temperature technique to establish kinetic parameters for solid-state decompositions using a vacuum microbalance. Thermochim Acta. 1978;24:293–306.
23. Arrhenius S. On the reaction rates of the inversion of cane sugar by acids. Z Physik Chem. 1889;4:226–48.
24. Wang Z, Jiao C, Hu Y. Thermal degradation kinetics of ethylene-vinyl acetate copolymer containing hydrotalcite and red phosphorus. Polym Plast Technol. 2008;47:771–8.
25. Khan N, Dollimore D, Alexander K, Wilburn FW. The origin of the exothermic peak in the thermal decomposition of basic magnesium carbonate. Thermochim Acta. 2001;367:321–33.
26. Hollingbery LA, Hull TR. The thermal decomposition of huntite and hydromagnesite—a review. Thermochim Acta. 2010;509:1–11.
27. Vágvölgyi V, Hales M, Frost RL, Locke A, Kristóf J, Horváth E. Conventional and controlled rate thermal analysis of nesquehonite $Mg(HCO_3)(OH)\cdot 2(H_2O)$. J Therm Anal Calorim. 2008;94:523–8.

28. Selvamani T, Yagyu T, Kawasaki S, Mukhopadhyay I. Easy and effective synthesis of micrometer-sized rectangular MgO sheets with very high catalytic activity. Catal Commun. 2010;11:537–40.
29. Selvamani T, Mukhopadhyay I. Preparations and characterization of basic magnesium carbonates using natural brine as precursor. Int J Mater Sci. 2009;4:641–8.
30. Koga N, Yamane Y. Effect of mechanical grinding on the reaction pathway and kinetics of the thermal decomposition of hydromagnesite. J Therm Anal Calorim. 2008;93:963–71.